A distributed real-time power management scheme for shipboard zonal multi-microgrid system

Xie, Peilin; Tan, Sen; Bazmohammadi, Najmeh; Guerrero, Josep M.; Vasquez, Juan C.; Matas, José; Mariachet, Jorge El

Published in:
Applied Energy

DOI (link to publication from Publisher):
10.1016/j.apenergy.2022.119072

Publication date:
2022

Document Version
Publisher's PDF, also known as Version of record

Applied Energy 317 (2022) 119072

Contents lists available at ScienceDirect

Applied Energy

journal homepage: www.elsevier.com/locate/apenergy

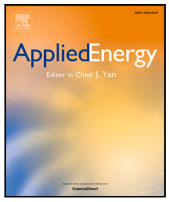

A distributed real-time power management scheme for shipboard zonal multi-microgrid system

Peilin Xie [a,*], Sen Tan [a], Najmeh Bazmohammadi [a], Josep. M. Guerrero [a], Juan. C. Vasquez [a], Jose Matas Alcala [b], Jorge El Mariachet Carreño [b]

[a] Center for Research on Microgrids (CROM), AAU Energy, Aalborg University, Aalborg, 9220, Denmark
[b] Department of Electronic Engineering, Universitat Politècnica Catalunya, Barcelona, 08019, Spain

ARTICLE INFO

Keywords:
Distributed PMS
Power management
Real-time management
Shipboard power system

ABSTRACT

The increasing demands of reducing fuel consumption for marine transportation have motivated the use of high fuel efficiency power plants and the development of power management systems (PMS). Current studies on shipboard PMS are mostly categorized as centralized, which are easy to be implemented and able to converge to the global optimum solutions. However, centralized techniques may suffer from the high computational burden and single-point failures. Considering the future trends of marine vessels toward zonal electrical distribution (ZED), distributed PMS are becoming an alternative choice. To achieve the ship high fuel-efficiency operation under high fluctuated propulsion loads, a real-time distributed PMS is developed in this paper that can acquire as good fuel economy as centralized PMS, but with faster computing speed. With a combination of filter-based, rule-based, and optimization-based approaches in a highly computationally efficient manner, the distributed PMS is constructed based on three layers that guarantees not only high fuel efficiency, but also sufficient energy reservation in different sailing modes and even in faulty conditions. Convergence tests and multiple case studies are conducted to prove the effectiveness of the proposed PMS in terms of fast convergence speed, improved fuel efficiency, and enhanced resilience.

1. Introduction

According to the International Maritime Organization study on greenhouse gas (GHG) emissions from ships, stringent regulations are applied that aim to reduce GHG emissions by 50% by 2050 [1]. Considering the fact that diesel fuel is still the major resource for all maritime applications, improving the fuel efficiency is of great importance and gaining a growing interest. One of the solutions is to replace the traditional gensets (fixed-speed diesel generators (DGs)) with high fuel efficiency equipment (variable-speed DGs, fuel cells, etc.) or alternative energy sources (wind turbine, photovoltaic panel, etc.). Among all, variable-speed DGs not only have high reliability, large capacity, and less financial investment, but also can save more fuel in an average range of 10% to 20%, even up to 40% at certain load conditions compared to the traditional fixed-speed DGs [2,3]. Thus, variable-speed DGs are gaining increasing interests especially in DC applications, thereby are selected as the main power supplier in this paper. Besides using highly fuel-efficient gensets and integrating renewable energy resources, developing efficient solutions for energy storage to provide an auxiliary power source for main gensets, and designing advanced power/energy management strategies to achieve economical and environmental-friendly operations are required.

Power and energy management system is an effective tool for facility sizing [4–6], early-stage energy dispatching [7–9], ship routine scheduling [8,10–12], demand-side management [13,14], and real-time power allocation. Although several PMSs have been developed for many other applications viz. terrestrial [15], residential [16], vehicle [17], and aircraft power systems [18], there are different challenges and specific requirements for PMS of shipboard power systems (SPSs). The biggest challenge is the composition of the loads. Different from terrestrial microgrids, ship propulsion loads take a large proportion of the onboard loads, which are affected largely by the sea states, season, wind, ship sailing mode, and so on. The disturbances from the environment and changes of cruising plans will result in uncertainties and fluctuations of the propulsion load, and thereby increasing the difficulty of load forecasting, as well as the energy/power management. Especially in extreme sea conditions, propulsion loads can severely fluctuate due to ventilation and in-and-out-of water effects. If not handled well, it will negatively affect both electrical and mechanical

* Corresponding author.
E-mail addresses: pxi@energy.aau.dk (P. Xie), sta@energy.aau.dk (S. Tan), naj@energy.aau.dk (N. Bazmohammadi), joz@energy.aau.dk (J.M. Guerrero), juq@energy.aau.dk (J.C. Vasquez), jose.matas@upc.edu (J.M. Alcala), jorge.el.mariachet@upc.edu (J.E.M. Carreño).

https://doi.org/10.1016/j.apenergy.2022.119072
Received 11 February 2022; Received in revised form 16 March 2022; Accepted 2 April 2022
Available online 26 April 2022

Nomenclature

β	Propeller loss factor
Δ	Value Changes over a sampling time
η_{chg}, η_{dis}	Constant values, referring to the efficiencies of battery during charging and discharging mode
η_{dg}	DG efficiency
λ	Regularization parameter
$\mathbb{N}_i$	The set of neighbors of zone i
μ_b	Constant penalty value of battery
ω	DG rotational speed
ρ	Augmented Lagrangian parameter
ρ_{water}	Sea water density
a_0, a_1, a_2, a_3, a_4	Fixed values by curve fitting
b_0, b_1, b_2, b_3	Fixed values by curve fitting
C	DG constant loss
c_0, c_1, c_2	Fixed values by curve fitting
C_{uc}	UC capacitance
D	Propeller diameter
ef_b	Equivalent factor of battery
h/D	Propeller submergence ratio
I_b	Battery current
I_{uc}	UC current
k_c	DG copper loss coefficient
K_i	Integral gain
k_i	DG iron losses coefficient
K_Q	Torque advance coefficient
k_w	DG windage losses coefficient
k_b	Penalty coefficient of battery
k_{dg}	On/off signal of DG
m_b	Equivalent fuel consumption of battery
m_{dg}	Fuel consumption of DG
m_{total}	Total equivalent fuel consumption
max	Upper limits
min	Lower limits
N	Number of zones
n_{dg}	Diesel engine speed
n_{prop}	Motor shaft speed
P_b	Output power of battery
P_{dg}	DG output power
P_{eng}	Output power of the diesel engine
$P_{i,j}$	Transmitted power from zone i to zone j
$P_{l.uc}$	Load demand for UC
P_{load}	Total ship loads
P_{prop}	Ship propulsion load
P_{loss_b}	Power loss of battery
$P_{loss_{uc}}$	Power loss of UC
$P_{lowfreq}$	Low-frequency load to be shared by DG and batteries
P_{uc}	Output power of UC
Q_b	Battery capacity
Q_{prop}	Ship propeller torque
R_b	Internal resistance of battery
R_{uc}	Internal resistance of UC
s	Index of ADMM iterations
$SFOC_{eq}$	Equivalent SFOC value of battery
$SOC_{b.desire}$	The desired SOC value
SOC_b	Battery SOC
SOC_{ref}	Reference SOC value of UC
SOC_{uc}	UC SOC
T	DG engine torque
T_f	DG friction losses coefficient
u	Control input vector
V_{oc}	Open-circuit voltage of battery
V_{uc}	Maximum voltage of UC
$z_{i,j}$	Local copy of $P_{j,i}$ in subsystem i
$z_{mid,ij}$	Middle value of the transmitted power between the neighboring zones
ADMM	Alternating direction method of multipliers
DG	Diesel generator
ECMS	Equivalent consumption minimization strategy
EF	Equivalence factor
ESS	Energy storage systems
GHG	Greenhouse gas
HESS	Hybrid energy storage systems
LC	Local controller
LPF	Low-pass filter
MPC	Model predictive control
PMS	Power management systems
SFOC	Specific fuel oil consumption
SOC	State of charge
SPS	Shipboard power systems
UC	Ultra-capacitor
ZED	Zonal electrical distribution
$P_{loss_{dg}}$	DG total loss
P_{LPF}	Load filtered by LPF

systems. For instance, increasing fuel consumption, risk of blackouts due to unpredictable power consumption, and maintenance cost due to unnecessary mechanical wear and tear [19].

To deal with problems arose by the high dynamic load condition, hybrid use of energy storage systems (ESSs) and real-time power management systems have been proved to be effective. In [20–23], a hybrid ESS (HESS) consisting of batteries and ultra-capacitors (UCs) is recommended, with UCs to supply pulse or high-frequency loads and batteries to provide auxiliary power for the main power supplier. While in [24], UC is replaced with a flywheel due to its higher power density and higher energy density. By use of different kinds of ESSs, dynamic load demand can be met while avoiding frequent charging and discharging of batteries, thereby extending service life and reducing maintenance cost. However, effectiveness of the HESS depends largely on the power management strategy, which splits power between main gensets and hybrid ESS based on different optimization goals.

Studies on real-time optimization-based power management of SPSs can be roughly categorized based on their optimization goals into minimization of fuel consumption [20–23,25–29], reduction of environmental footprint [28,30–32], and minimization of total economic investment [30,31,33–35]. Better knowledge of future load profile leads to better optimization results. Some studies, for example, [23,25,26,36] use equivalent consumption minimization strategy (ECMS) to calculate the instantaneous equivalent fuel consumption of ESS and determine the optimal power split. One major advantage of the ECMS is that it does not require the knowledge of future loads, thereby is easy to be implemented. Other studies, such as [20–22,24], form the operation management problem of SPSs in the framework of model predictive control (MPC). The effectiveness of MPC depends largely

on the knowledge of the system model, future loads, as well as the prediction horizon. Authors in [22,37] develop the mathematical model of propulsion-load fluctuations for future load prediction and authors of [38] combine linear prediction with input observer. However, these strategies are tuned with a limited number of load profiles. To meet all load types without prior knowledge of future information, authors in [30] use an intelligent method, Double Q reinforcement learning, to predict future load with zero-knowledge of future voyages. However, a more precise load forecasting requires more historical load information, bigger computing effort for load prediction, a longer prediction horizon in case of MPC, and more computation time. Thus, it might be difficult to use them in real-time applications, especially for large-scale shipboard systems.

Another major concern of the above-mentioned works is that they are mostly developed in centralized arrangement, which requires knowledge of the entire power system. Despite the benefit of a centralized arrangement in obtaining globally optimal results, it requests a large amount of computational resources and may have the risk of single-point failures. Due to the advantages in low computational consumption, communication robustness, and privacy preservation [39,40], PMS in distributed arrangement is drawing attention and is therefore mainly considered in this paper. Besides, zonal electrical distribution systems for marine vessels are becoming a future trend due to lower acquisition costs, lower weight, high quality of power supply, and better operational flexibility [41], which presents opportunities for the development and application of PMS in a distributed arrangement.

Although there exist several studies dedicated to either distributed control of SPSs or operation management of ZED-based ships, distributed operation management of ZED systems has not reached fruition so far [42]. Regarding distributed power and energy management systems, authors of [43] solve the coordination problem of the ESS and power generators while considering pulsed loads. In [44], a continues power supply with minimum voltage violation is achieved by developing a power and energy management strategy in multiple layers. However, neither of these studies are designed for ZED-based shipboard power systems. Authors in [45,46] use multi-agent technology to realize the demand-side management and ensure a maximum generation support for ZED-based ships. In [47–49], distributed algorithms such as distributed-MPC and multi-agent system are used to maintain the power balance, keep ESS energy reservation, and reduce the power losses. In [50], decentralized PMS is used to enhance the system resilience by introducing the concept of cloud energy storage system to a shipboard power system. One problem of the current researches is that most of them focus on the demand-side management or maintaining power balance under presence of pulsed loads. However, issues related to propulsion load fluctuations still exist, which results in many other problems such as power imbalances, increased fuel consumption, insufficient energy reservations, and difficulties with zonal cooperation and communications. Considering that most ZED-based ships are large-scale, if traditional centralized PMSs are simply applied to ZED-based SPSs, several issues might raise. For instance, the presence of multiple energy resource types, increased amount of information, and complex power flows increase the complexity of centralized PMSs and make them inapplicable for real-time applications. Therefore, there is an urgent need to study distributed real-time PMSs for efficient power splitting under propulsion load fluctuation with fast computing speed, high reliability, and good performance.

In this paper, a real-time distributed power allocation strategy for ZED-based SPSs in the presence of load fluctuations is proposed. ECMS is chosen for its advantages of fast calculations, zero requirement for future load information, and satisfactory performance in terms of fuel savings. In addition, for the sake of saving computing effort, a filter-based control system is developed to exclude the UC operation from the optimization process, and forcing it to support only high-frequency load components. Unlike previous works where the output of UC is calculated at every sampling time even in extremely fluctuating load conditions, the filter-based control allows faster calculation and faster reactions in case of facing sudden load changes. The main goal of this paper is to solve the real-time power allocation problem for ZED-based shipboard power systems in the presence of load fluctuations. There are mainly two objectives: (i) achieving highly fuel-efficient operation, (ii) maintaining a secure state of charge (SOC) level of HESS during the voyage. The contributions of this paper are summarized below:

1. A novel three-layer real-time distributed PMS framework is developed that provides a simple way for splitting power between the main power suppliers and the HESS while maintaining a high fuel efficiency. In the meanwhile, energy reservation can be well maintained for the hybrid ESS during the voyage.

2. The proposed distributed PMS scheme allows each zone to focus on its own operation management problem with the knowledge of local load and limited neighbor information to achieve an overall improvement in fuel efficiency and computing speed. Neighbor zones are also able to support each other in the case of single-point failure in one zone, resulting in a more reliable and resilient operation.

3. The simple structure and fast convergence speed makes the developed PMS suitable for real-time applications and can be easily applied to other marine applications as well.

4. The fuel saving ability, computing speed, and fault supporting capability of the proposed PMS is evaluated and discussed under different normal and faulty operating scenarios considering failure of DGs and interconnection links of neighboring zones.

This paper is organized as follows. In Section 2, the ship structure is described and the electrical components are modeled. The proposed distributed PMS is presented in Section 3. The case studies are investigated under two scenarios and discussed in Section 4. Finally, conclusion is given in Section 5.

2. SPS description and modeling

The DC SPS studied here is ZED-based that is divided into four zones according to the physical location of components. Fig. 1 shows the overall structure of the SPS and distributed PMS scheme. All zones have a similar composition, consisting of variable-speed DG as the main power supplier and HESS (ultra-capacitors and batteries) as auxiliary sources, but with different load types. The main loads for the first and fourth zones are the propulsion load while for the middle zones are the ship service loads. The local controller (LC) gathers local and neighbors' information to determine the optimal power allocation inside the zone and power transmissions between the zones. Updated information are also sent to the adjacent neighbors to realize the consensus on the exchanged power. Therefore, each zone is able to supply its local load demand and provide auxiliary support to its neighbors in a fuel-efficient and safe manner. The modeling of each component is given in the following sub-sections.

2.1. Diesel generator

Variable-speed DG is utilized here as the main power suppler due to its advantage of higher fuel efficiency. The optimal specific fuel oil consumption (SFOC) characteristics of variable-speed DGs are shown in Fig. 2 [51,52]. The optimal operational speed is different for different load conditions, as can be seen from the blue line. And the corresponding SFOC values can be found by checking the black line. As can be seen, DGs have a low fuel efficiency at low load conditions. The optimal fuel-efficient loading range is between 60% and 80% and the corresponding rotational speed is between 1200 *rmp* and 1400 *rmp*. By curve fitting, the output power of the diesel engine (P_{eng}) can be expressed as a nonlinear function of the engine speed (n_{dg}),

$$P_{eng} = a_0 + a_1 n_{dg} + a_2 n_{dg}^2 + a_3 n_{dg}^3 + a_4 n_{dg}^4 \quad (1)$$

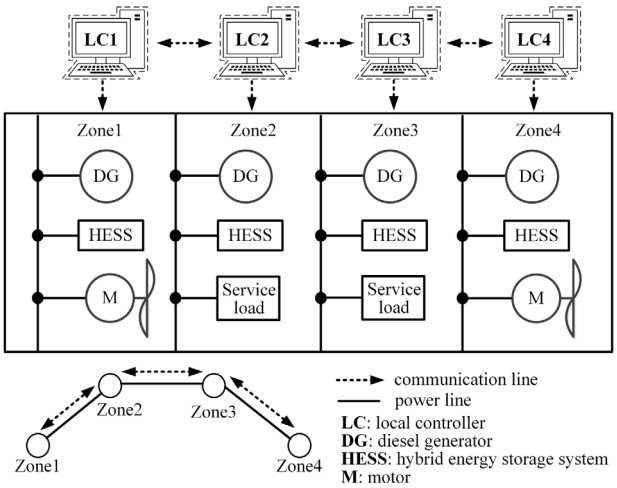

Fig. 1. The topology of the ZED-based SPS.

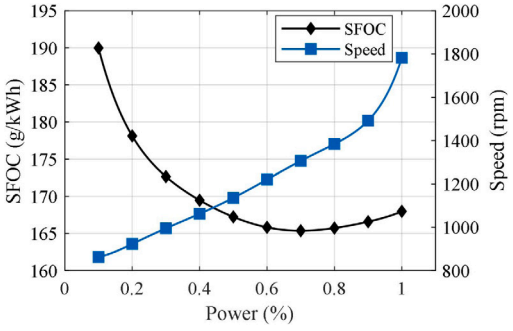

Fig. 2. SFOC and speed characteristics of the DGs.

where a_0, a_1, a_2, a_3, a_4 are fixed values, and are set by curve fitting to -1.93×10^{7}, 5.7098×10^{4}, -63.97, 0.0333, and -6.5138×10^{-6} respectively. Furthermore, the SFOC curve is determined as follows,

$$SFOC = \begin{cases} b_0 + b_1 n_{dg} + b_2 n_{dg}^2 + b_3 n_{dg}^3 & n_{dg} <= 1340 \\ c_0 + c_1 n_{dg} + c_2 n_{dg}^2 & n_{dg} > 1340 \end{cases} \quad (2)$$

where b_0, b_1, b_2, b_3 are set by curve fitting to 620.6534, -0.9737, 6.8199×10^{-4}, and -1.5574×10^{-7}, respectively. And c_0, c_1, c_2 are set to 135.98, 0.03, and -8.81×10^{-6}.

The diesel engine provides torque to the generator, and the generator converts that torque into electrical energy. Due to the electrical losses including copper losses (k_c), iron losses (k_i), friction losses (T_f), windage losses (k_w), and constant losses (C) [53], the output power of the diesel generation system (P_{dg}) can be determined as,

$$P_{dg} = P_{eng} - P_{loss_{dg}} \quad = P_{eng} - (k_c T^2 + k_i \omega + T_f \omega + k_w \omega^3 + C) \quad (3)$$

2.2. Hybrid energy storage system

Due to the high energy density, ultra-capacitors are able to deliver energy faster than batteries and thus capable of supplying high-frequency loads. However, the energy capacity of commercially available UCs is smaller than batteries of the same size [54]. From security and economy points of view, batteries and UCs provide a promising hybrid storage solution and thereby are utilized in this paper. The state-space equation of the HESS can be defined as [22],

$$\begin{bmatrix} \dot{SOC}_b \\ \dot{SOC}_{uc} \end{bmatrix} = \begin{bmatrix} 1/(3600Q_b) & 0 \\ 0 & -1/(V_{uc}C_{uc}) \end{bmatrix} \begin{bmatrix} I_b \\ I_{uc} \end{bmatrix} \quad (4)$$

where SOC_b and SOC_{uc} are the SOC of the battery and UC, I_b and I_{uc} are the battery and UC currents, Q_b is the battery capacity, V_{uc} is the maximum voltage of the UC, and C_{uc} is the UC capacitance.

Taking the power losses into account, the output power of battery (P_b) and UC (P_{uc}) can be expressed as follows,

$$P_b = V_{oc} I_b - P_{loss_b} = V_{oc} I_b - R_b I_b^2 \quad (5)$$

$$P_{uc} = V_{uc} SOC_{uc} I_{uc} - P_{loss_{uc}} = V_{uc} SOC_{uc} I_{uc} - R_{uc} I_{uc}^2 \quad (6)$$

where V_{oc} is the open-circuit voltage of the battery, which is assumed to be constant for simplicity, considering the short sampling time and the small variation of SOC. P_{loss_b} and $P_{loss_{uc}}$ are the power losses caused by internal resistance R_b and R_{uc} of battery and UC respectively.

2.3. Propeller and ship hydrodynamic

According to [55], propulsion load fluctuation mainly includes two parts: low-frequency fluctuations caused by the periodical sea waves, and high-frequency fluctuations caused by propeller motion in-and-out-of water. The propulsion load can be derived from the propeller model and the hydrodynamic model. The propeller torque (Q_{prop}) and mechanical power (P_{load}) can be formulated as nonlinear functions of motor shaft speed (n_{prop}), environmental parameters (e.g. water density (ρ_{water}), wave period), and propeller parameters (e.g. propeller diameter (D), pitch ratio, submergence (h), and advance coefficient (K_Q) and can be expressed as [55],

$$Q_{prop} = sign(n_{prop}) \beta \rho_{water} n_{prop}^2 D^5 K_Q \quad (7)$$

$$P_{prop} = 2\pi n_{prop} Q \quad (8)$$

where β is the propeller loss factor referring to the effects of propeller motion in-and-out-of water that is dependent on the submergence ratio (h/D) as follows [56,57],

$$\beta = \begin{cases} 0 & h/D < -0.48 \\ 1 - 0.675 \times (1 - h/D)^{1.258} & -0.48 \le h/D \le 1.3 \\ 1 & h/D > 1.3 \end{cases} \quad (9)$$

The high dynamics of h/D is the main reason of propulsion loads fluctuations that is usually modeled as a sine wave. In this paper, load fluctuations of up to 2 Hz are investigated. More details will be provided in Section 3.

2.4. Ship service loads

The ship service load refers to the electricity consumption of various onboard equipment, including the onboard lighting system, navigation system, air conditioning and so on [58]. Different from the propulsion load which can be highly fluctuating, periodical, and changeable, ship service loads have more specific load profiles for certain times of the day and are always considered as a series of step load changes for simplification as in [58–60] and in this paper as well.

3. Distributed power management strategy

In this paper, a novel real-time distributed power management strategy is developed to acquire a highly fuel-efficient operation and maintain a secure SOC level of HESS. All zones have a similar PMS structure. A typical zonal PMS configuration for Zone 1 is taken as an example and shown in Fig. 3. The proposed PMS structure contains three parts: the UC control layer, the DG control layer, and the distributed optimization layer. The three layers work in sequence to distribute the high-frequency load to UCs and allocate the low-frequency load to the DG and batteries.

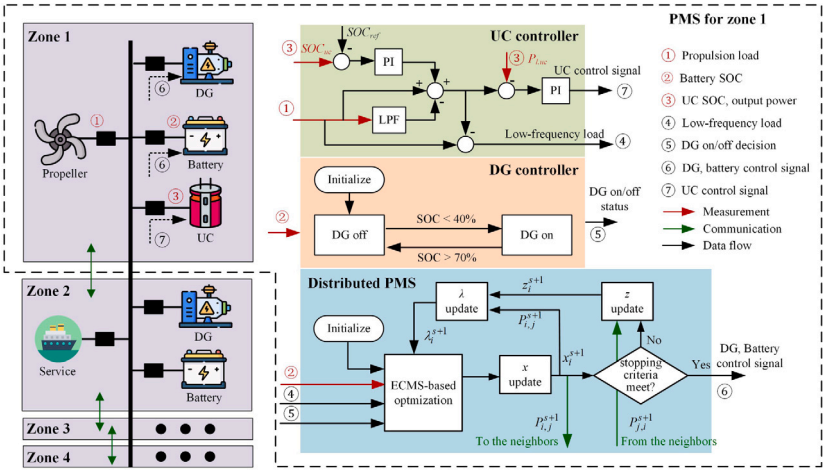

Fig. 3. The proposed distributed PMS scheme.

3.1. UC controller

To reduce the stress of the propulsion load fluctuations, filter-based control strategies have been proven to be effective in combination with HESS [21,61]. To avoid the negative effect of large time lags caused by high-pass filters on high-frequency loads, a low-pass filter (LPF) is utilized here to separate the load fluctuation into low-frequency and high-frequency components.

In the most of the previous works, the SOC of UCs is not considered, leaving a risk of over-charging or over-discharging. To maintain a healthy level of SOC, a PI controller is used to maintain the SOC at an acceptable level. The total amount of load meant for UCs ($P_{l.uc}$) is the sum of filtered high-frequency loads and the power required for maintaining its SOC level. As can be seen in Fig. 3, the total load demand for UCs is expressed as:

$$P_{l.uc} = P_{load} - P_{LPF} + (SOC_{uc} - SOC_{ref})(K_i + K_p/s) \tag{10}$$

And the low-frequency load to be shared by DG and batteries is calculated by:

$$P_{lowfreq} = P_{load} - P_{l.uc} \tag{11}$$

3.2. DG controller

This layer is built based on a series of simple rules to decide the on/off status of the local DG as shown in Fig. 3. According to the local load information ($P_{lowfreq}$) from the upper layer and the current SOC of local batteries, the controller turns on the DG at high load conditions or low SOC levels and switch it off in other conditions. By doing so, low-load operation of DG can be avoided, and over-charging or over-discharging of batteries can also be prevented. The on/off signal of DG (k_{dg}) is then sent to the next layer for the optimization process.

3.3. Distributed optimization

By gathering the load information ($P_{lowfreq}$) from the first layer, the DG on/off signal (k_{dg}) from the second layer, and the measured battery SOC value, this layer decides the optimal power allocation between the local DG and batteries by solving the instantaneous optimization problem. The optimization problem is built based on equivalent consumption minimization strategy, and is solved in a distributed way by alternating direction method of multipliers (ADMM) technique.

3.3.1. Optimization problem formulation

The optimization problem is developed based on ECMS, an effective energy management technique capable to solve the instantaneous power splitting problem. The basic concept of ECMS is that the ESS can be seen as auxiliaries for the DGs. The energy discharged from ESS will eventually be charged later. So the amount of fuel consumed for charging the ESS is equivalent to the fuel consumption during ESS discharging. Based on this idea, if we regulate the charging/discharging of ESS according to the SOC condition and current load information, DG can be operated at a high fuel-efficiency point. The cost function is the combination of fuel consumption of DG and equivalent fuel consumption of ESS [36]. The equivalent accuracy depends on the equivalence factor (EF), which stands for the conversion relationship between the electrical power consumption and fuel consumption, and needs to be determined carefully [62,63]. To simplify the calculation, most of researches simply consider the EF as a constant [64]. Despite its advantages of simplifying implementation, it may fail to capture the real transformation relationship, thus lead to unsatisfactory results. So, in this paper, the EF is adjusted in real-time according to the current SOC level. Although more computational effort might be required, more accurate equivalent fuel conversion can be expected.

The system equivalent fuel consumption (m_{total}) is the sum of generator fuel consumption (m_{dg}), and converted equivalent fuel consumption of the battery (m_b),

$$m_{total}(t) = k_{dg} \cdot m_{dg}(t) + m_b(t) \tag{12}$$

where m_{dg} can be calculated by,

$$m_{dg}(t) = SFOC \cdot P_{dg}(t)/(\eta_{dg} \cdot 3.6 \cdot 10^6) \tag{13}$$

in which η_{dg} is the DG efficiency. In (12), m_b can be expressed as follows,

$$m_b(t) = ef_b(t) \cdot SFOC_{eq} \cdot P_b(t)/(3.6 \cdot 10^6) \tag{14}$$

where ef_b is the equivalence factor of the battery, and $SFOC_{eq}$ sets a reference fuel consumption value for the ESS. It is worth noticing that if the equivalent fuel cost $SFOC_{eq}$ is set too low, ESS is encouraged to be charged, because the energy in the ESS is considered cheaper than the DG. While a high value will discourage battery usage due to the high recharge costs. Considering the additional transfer and conversion losses during the charging/discharging process and the high fuel-efficiency of variable-speed DGs under high load conditions, the $SFOC_{eq}$ here is set the peak value of SFOC in Fig. 2 such that it can encourage the DG to provide more power, thus avoiding low loading operating conditions.

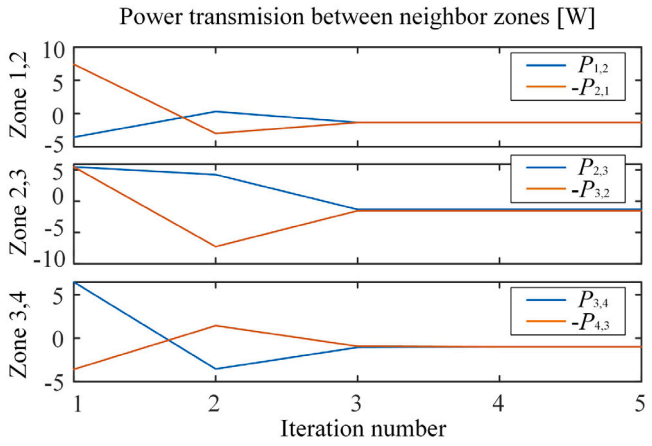

Fig. 4. The convergence performance for one sampling instance.

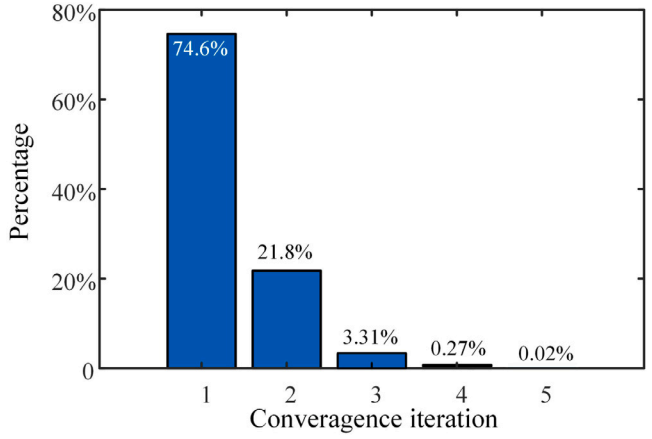

Fig. 5. Overall convergence rate over 70000 samples.

The equivalence factors of battery (ef_b) can be derived as [65],

$$ef_b(t) = \begin{cases} \dfrac{k_b}{\eta_{dg} \cdot \eta_{dis}} & P_b \geq 0 \\ \dfrac{k_b \cdot \eta_{chg}}{\eta_{dg}} & P_b < 0 \end{cases} \tag{15}$$

where η_{chg} and η_{dis} are constant values, referring to the charging and discharging efficiencies of the battery, respectively. Furthermore, k_b is the penalty coefficient of the battery. The key point of this parameter is to keep the SOC around a healthy level ($SOC_{b.desire}$), and is expressed as,

$$k_b = 1 - \mu_b \frac{SOC_b - SOC_{b.desire}}{SOC_{b.desire}} \tag{16}$$

where μ_b is a constant value that is set to 1.2 in this paper. Besides, $SOC_{b.desire}$ represents the desired level of SOC and is set to 50%. The penalty coefficient varies with the change of SOC level to keep the ESS at a predefined level. For example, if the battery SOC is greater than $SOC_{b.desire}$, a cheaper cost is considered for the energy stored in the battery to encourage battery discharging and vice versa. In this way, a healthy SOC and reliable energy backup is maintained.

In this paper, the goal of the operation management is to minimize the system fuel consumption in real time, therefore the optimization problem at time t_k is formulated as,

$$\min_{u_i(t_k)} \quad J = \sum_{i=1}^{N} m_{i,total}(u_i(t_k)) \tag{17}$$

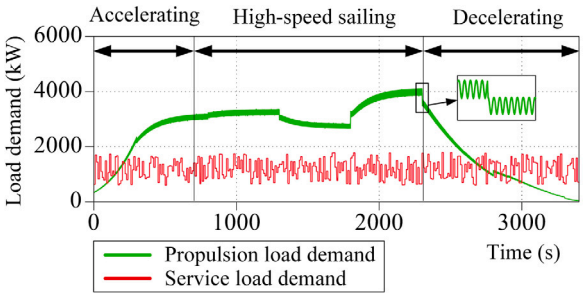

Fig. 6. Propulsion and service load profiles.

with a set of equality and inequality constraints,

$$\begin{aligned} & P_{i,dg}(t_k) + P_{i,b}(t_k) = P_{i,lowfreq}(t_k) + \textstyle\sum_{j\in\mathbb{N}_i} P_{i,j}(t_k) \\ & P_{i,j}(t_k) + P_{j,i}(t_k) = 0, \forall j \in \mathbb{N}_i \\ & n_{i,dg}(t_k) \in [n_{dg.min}, n_{dg.max}] \\ & I_{i,b}(t_k) \in [I_{b.min}, I_{b.max}] \\ & SOC_{i,b}(t_k) \in [SOC_{b.min}, SOC_{b.max}] \\ & P_{i,j}(t_k) \in [P_{i,j.min}, P_{i,j.max}] \\ & \Delta n_{i,dg} \leq \Delta n_{dg.max} \\ & \Delta I_{i,b} \leq \Delta I_{b.max} \\ & \Delta SOC_{i,b} \leq \Delta SOC_{b.max} \end{aligned} \tag{18}$$

where $u = [n_{dg}, I_b]^T$ is the control input vector. N is the number of zones that is considered equal to 4 in this paper. The set of neighbors of zone i is represented by $\mathbb{N}_i$. Besides, $P_{i,lowfreq}$ is the low-frequency load demand of zone i and $P_{i,j}$ is the transmitted power from zone i to zone j. The first equality constraint ensures that the load demand is met at every step, while the second constraint is related to the power exchange between neighboring zones. The inequality constraints include the DG rotation speed limit, the ESS currents limit, the ESS SOC limit, the exchanged power limit, and the limits of their changing rate. Subscript *min* and *max* refers to the lower and upper limits, and Δ shows the changes over a sampling time.

3.3.2. Algorithm development

In the optimization problem (17) and (18), the local constraints apply only to the local zones while the global objective is the composition of the objectives of all individual zones. The only coupling is imposed by the interaction equality constraints. Since there is no master controller, the joint optimization problem needs to be solved in a distributed way. Among the distributed algorithms, the ADMM is widely used as it can break convex optimization problems into smaller problems and finds the best performance [66]. Based on ADMM, the decoupling and solving algorithm is developed.

To decouple the interaction constraints, a new variable $z_{i,j}$ is defined for each zone i:

$$z^s_{i,j} - P^s_{j,i} = 0, \forall j \in \mathbb{N}_i \tag{19}$$

where $z_{i,j}$ is the local copy of $P_{j,i}$ in subsystem i and s is the index of ADMM iterations. To reach an agreement on the neighbors' power exchange value, another variable is defined,

$$z^s_{mid,ij} = \frac{1}{2}(P^s_{i,j} - z^s_{i,j}) \tag{20}$$

where $z_{mid,ij}$ is defined as the middle value of the transmitted power between the neighboring zones.

The local optimization problem is therefore given by minimization of the augmented Lagrangian function:

$$\min_{u_i^{s+1}, P_{i,j}^{s+1}} L_i(u_i^s, P_{i,j}^s, \lambda_i^s) = J_i(u_i^s) + \sum_{j\in\mathbb{N}_i} (\lambda_i^s (P_{i,j}^s - z_{mid,ij}^s) + \frac{\rho}{2} \| P_{i,j}^s - z_{mid,ij}^s \|_2^2) \tag{21}$$

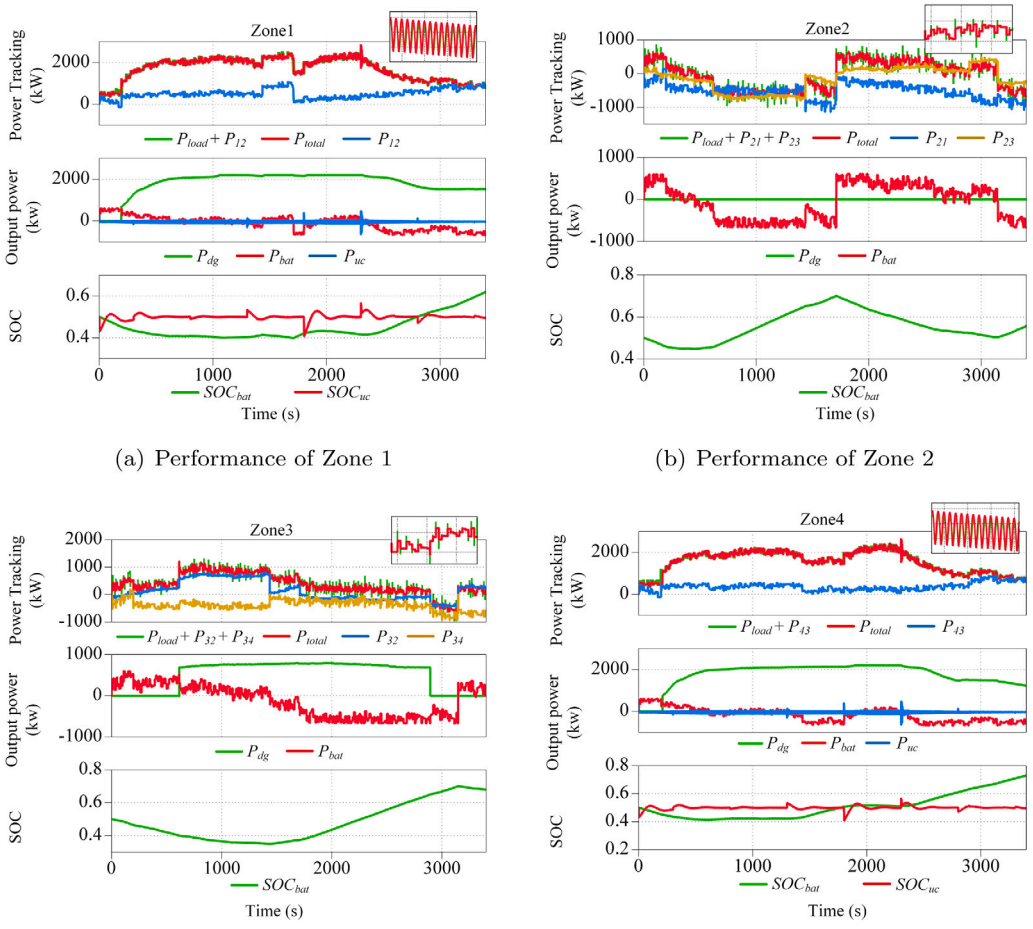

(a) Performance of Zone 1 (b) Performance of Zone 2

(c) Performance of Zone 3 (d) Performance of Zone 4

Fig. 7. Performance of each zone for an one-hour cruise.

Algorithm 1 shows the procedure of the developed algorithm based on ADMM technique to solve the optimization problem in a distributed manner.

Algorithm 1

For each subsystem i:
Initialize $u_i, P_{i,j}, z_{i,j}$,
Repeat
  Initialize λ_i
  for $s = 1, 2, \cdots, k$
  solve the optimization problem $(u_i^{s+1}, P_{i,j}^{s+1}) = argminL_i$
  send $P_{i,j}^{s+1}$, receive $P_{j,i}^{s+1}$
  compute $z_{i,j}^{s+1}$ and $z_{mid,ij}^{s+1}$ based on Eq. (19) and Eq. (20)
  compute $\lambda_i^{s+1} = \lambda_i^s + \rho(P_{i,j}^{s+1} + z_{i,j}^{s+1})$
Until stopping criteria checked:
  (maximum iterations or minimum convergence tolerance)

Through this iterative gradient ascent method, ADMM finds the dual optimum. In each iteration, the evaluation of the dual function is split into two consecutive steps where first the Lagrangian function is minimized over u_i and $P_{i,j}$ and next $z_{mid,ij}$ is updated. In this way, $P_{i,j}$ and $z_{i,j}$ variables converge to the exact opposite value after several iterations and an agreement is reached. Fig. 4 presents the convergence performance for the proposed ADMM algorithm over a certain sampling time and Fig. 5 shows the convergence rate over 70000 samples. Due to the small amount of data required for transmission, the results show fast convergence properties, which can be achieved within 5 iterations. Around 74.6% of the cases converged in just one iteration, which largely reduces the computational time and effort.

4. Case studies

The purpose of case studies is to test the fuel saving ability, computing speed, and fault supporting capability of the proposed PMS. The simulation is implemented in MATLAB/Simulink 2018b, and the sampling time is set to 0.05 s. According to the convergence test in the last section, the maximum iteration is set to 5. And to avoid unnecessary computing efforts, the convergence tolerance is set to 0.5, computed by $(P_{i,j}^{s+1} + z_{i,j}^{s+1})$. Information of ship operation and load profiles are related to a 4500DWT Platform Supply Vessel [67]. Detailed ship parameters can be found in Table 1. Parameters for a single DG, battery, and UC are tabulated in Table 2. And the number of components for each zone is given in Table 3. The simulations include two scenarios: normal and faulty operating conditions. Simulation results of each scenario are discussed in the following parts.

4.1. Scenario 1: Normal operating condition

The profiles for the ship propulsion and service loads are shown in Fig. 6. For this one-hour cruise, the ship goes through three sailing modes. During the first 10 min, the ship speeds up from 0 to 12 knots. After that, there are 30 min of high-speed sailing with several occasional speed changes. The ship returns to port and decelerates to stop at the last 20 min. Due to the influence of sea waves and propeller in-and-out-of water behavior, the propulsion load would be periodical and highly fluctuating, as seen in green curve in Fig. 6. The studied ship comprises two propulsion motors, whose load demand is supported by

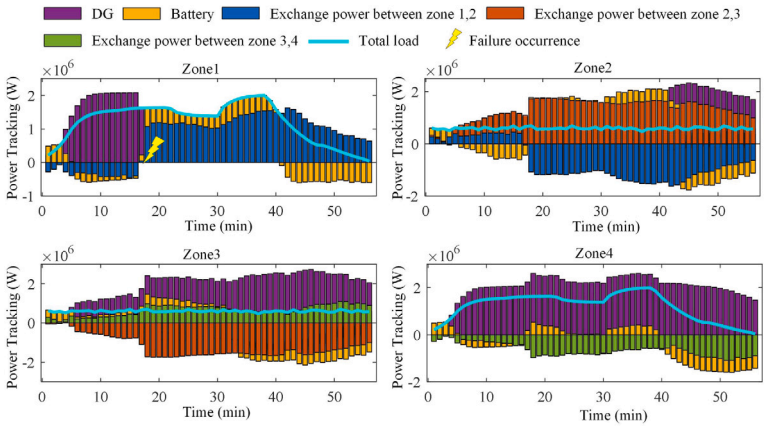

Fig. 8. Case 1: DG failure. DG1 fails at $t = 1000$ s.

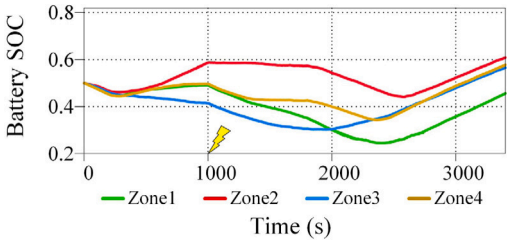

Fig. 9. Case 1: Battery SOC under DG failure condition.

Table 1
Ship and hydrodynamic parameters.

Parameters	Symbol	Value
Water density	ρ_{water}	1.025 g/cm^3
Number of blades	Z	4
Propeller diameter	D	5.6 m
Ship mass	m	2×10^4ton
Added mass	m_x	3×10^4 ton
Thrust deduction coefficient	t_d	0.2s
Frictional resistance coefficient	C_f	0.0043
Wave-making resistance coefficient	C_W	0.0043
Wind resistance coefficient	C_{air}	0.8
Ship wetted area	S	12300 m^2
Advance facing area in the air	A_t	675 m^2

Table 2
Electrical module parameters.

Modules	Parameters	Symbol	Values
Diesel generator	Rated power	P^*_{dg}	2 MW
	Efficiency	η_{dg}	96%
	Rotation speed limits	$n_{dg.min/max}$	900-1800
Battery	Rated power	P^*_b	37.5 kW
	Capacity	Q_b	500 Ah
	Voltage	V_{oc}	125 V
	Initial SOC	$SOC_{b.init}$	0.5
Ultra-capacitor	Rated power	P^*_{uc}	25 kW
	Capacitance	C_{uc}	63 F
	Resistance	R_{uc}	6.8 mΩ
	SOC Range	$SOC_{uc.min/max}$	0.2, 0.9
	Initial SOC	$SOC_{uc.init}$	0.5

Table 3
Installed components for each zone.

	Modules	Zone1	Zone2	Zone3	Zone4
Number	DG	1	1	1	1
	Battery	10	10	10	10
	UC	10	0	0	10

Table 4
Performance comparison between three different PMS arrangement.

Type	Fuel cost (kg)	Final SOC				Computing time (ms)
		Zone1	Zone2	Zone3	Zone4	
Centralized	632.4	0.6	0.542	0.542	0.6	6.9
Distributed	637.1	0.573	0.525	0.551	0.540	5
Decentralized	672.6	0.53	0.57	0.57	0.53	4

Zone 1 and Zone 4. The two middle zones are responsible for the ship service load, whose profile is shown in the red curve in Fig. 6.

Fig. 7 gives the simulation results of power tracking performance, zonal exchanged power, power splitting, and the SOC of HESS for each zone under the proposed power management strategy. It can be observed that the highly fluctuating part of propulsion load is well supported by UCs, while the low frequency part and the ship service load are shared between DGs and batteries. The initial state of all DGs is off. Due to the higher load demand in Zone 1 and Zone 4, their DGs are first turned on to meet the local load demand and also support their neighbors. In this way, low-load operating condition is avoided. With the increase of propulsion loads, both generators reach their maximum power but still cannot satisfy all the load demand. Hence, batteries are discharged as we can see decrease of batteries SOC before $t = 700$ s. To prevent discharging of the batteries, the local DG of Zone 3 is turned on and start to feed the remaining load demand and charge the batteries. As the propulsion loads decrease at the end of cruise, DGs reduces their output power and are shut down when batteries are charged. During this one-hour voyage, local load demands are all satisfied, and neighboring zones are allowed to support each other after evaluating their generation and loading condition. DGs are prevented from working in low-load operating points, which results in high fuel efficiency. In addition, a secure SOC level of HESS can be obtained in the range of 35%–70%, ensuring sufficient energy backup.

Regarding fuel saving and computing speed, a comparison between the proposed distributed PMS, traditional centralized PMS, and decentralized PMS is provided in Table 4. At the end of the cruise, all three techniques should reach the same SOC level to have a fair comparison.

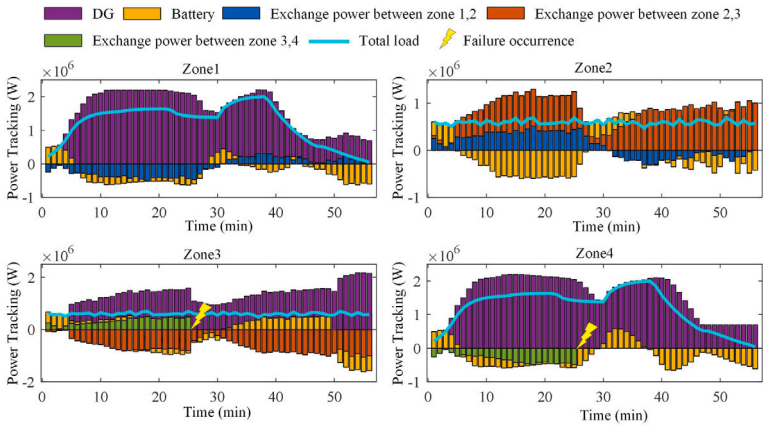

Fig. 10. Case 2: Disconnection of zones. Zone 3 and Zone 4 are disconnected at $t = 1500$ s.

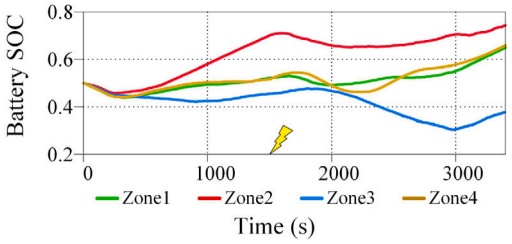

Fig. 11. Case 2: Battery SOC under disconnection of zones.

According to the results, centralized PMS achieves the optimal performance in fuel savings, but takes the longest computing time. That is reasonable because better knowledge of the system information leads to better optimization results but requires more effort in dealing with information. Decentralized PMS has the fastest computing speed but consumes the most fuel. Among all, the performance of the proposed distributed PMS is almost as good as the centralized PMS, while the computation time is reduced by 28%. Moreover, comparing with the decentralized PMS, 5.3% fuel saving can be achieved by applying the proposed technique.

4.2. Scenario 2: Faulty operating conditions

A major advantage of the proposed PMS is the enhanced resilience of the SPS under faulty operating conditions. The zonal communication and cooperation allow the neighbors to support each other when there is a fault in the system. To test the fault tolerance ability, two different failure conditions are studied in this section: DG sudden fault and disconnection of zones.

4.2.1. Case 1: DG failure

In this case, it is assumed that the DG in Zone 1 has a sudden failure and is shut down at $t = 1000$ s. The system performance is presented in Fig. 8, in which the exchanged power between neighboring zones is marked with the same color. For example, the transferred power from Zone 1 to Zone 2, and from Zone 2 to Zone 1 are represented with blue color. Positive values represent absorbing power from adjacent zones while negative values are related to sending power.

Before the failure occurs, DGs in Zone 1, Zone 3, and Zone 4 are in working mode, while Zone 2 relies on the support from Zone 1 and Zone 3 to meet the local load demand. After the failure occurrence, Zone 1 loses its main power sources and starts absorbing power from Zone 2, that is when we can observe a sudden rise of the exchanged power (blue). Due to the sudden power request from Zone 1, Zone 2 also faces power shortage and starts absorbing power from Zone 3 (orange), forcing the DG of Zone 3 to increase its generation. Zone 4 also helps to handle this emergency situation and provides additional power support. From Figs. 8 and 9, it can be observed that not only the load demands are met for each zone, but all batteries SOCs are kept at a healthy level. And at the end of the voyage, all batteries are charged to a high SOC level, which guarantees a sufficient energy backup for the future cruises.

4.2.2. Case 2: Disconnection of the neighboring zones

In this case, we assume that Zone 3 and Zone 4 suffer from an electrical and communication disconnection at $t = 1500$ s. As seen in Fig. 10, before the fault occurrence, the DG in Zone 4 is generating additional power to support the other zones. After disconnected from the system, Zone 4 operates in islanded mode and a decrease in DG generation and an increase in battery charging power can be observed. Through this adjustment on power scheduling, Zone 4 can preserve its stability after being disconnected. In other zones, due to the slow dynamics of DGs, batteries respond faster and are temporally discharged to compensate for the loss of support from Zone 4. DGs gradually increase their generation to supply the load and charge the batteries. Eventually, power balance of the zones is obtained. From Fig. 11, batteries of all zones are prevented from being over-discharged and are charged back at the end of the voyage. Accordingly, a healthy level of SOC is maintained while low-load operating conditions are avoided, thereby enabling more fuel-efficient operation.

Overall, the case studies under two scenarios confirm the effectiveness of the proposed PMS. The simulation results demonstrate that the proposed PMS ensures a highly fuel-efficient operation and power allocation within each zone and cooperation of adjacent zones. The proposed distributed method guarantees the system reliability under single-point failure and reduces the computational effort as well.

5. Conclusion

The high quality, flexible operation, and continuity of supply characteristics of ZED-based ships make them a viable alternative for marine transportation. In this paper, a real-time distributed PMS scheme was presented to maximize the fuel efficiency of ZED-based ships and guarantee a secure storage level and stable system operation under the presence of fluctuating propulsion loads.

To do so, a hybrid energy storage system was considered consisting of ultracapacitors to support high-frequency load fluctuations and batteries to provide auxiliary power to the main diesel generator. Besides, a three-layer distributed PMS framework was designed. The proposed method allows each zone to handle its local operation with limited information exchange with its neighboring zones, thus ensuring a faster computing speed and requiring less computational effort. The fast convergence speed and simple structure of the proposed method

make it suitable for real-time power scheduling. Furthermore, it can be easily implemented in other ZED-based ship applications. Simulation results validated the effectiveness of the proposed strategy in terms of fuel-saving and system resilience under normal and faulty operating conditions.

CRediT authorship contribution statement

Peilin Xie: Conceptualization, Methodology, Software, Investigation, Writing – original draft, Writing – review & editing. **Sen Tan:** Software, Writing – review & editing. **Najmeh Bazmohammadi:** Supervision, Writing – review & editing. **Josep. M. Guerrero:** Supervision, Project administration, Funding acquisition. **Juan. C. Vasquez:** Supervision, Project administration, Funding acquisition. **Jose Matas Alcala:** Supervision, Project administration. **Jorge El Mariachet Carreño:** Supervision, Project administration.

Declaration of competing interest

The authors declare that they have no known competing financial interests or personal relationships that could have appeared to influence the work reported in this paper.

Acknowledgment

This work was supported by VILLUM FONDEN, Denmark under the VILLUM Investigator Grant (no. 25920): Center for Research on Microgrids (CROM), www.crom.et.aau.dk.

References

[1] Armellini A, Daniotti S, Pinamonti P, Reini M. Evaluation of gas turbines as alternative energy production systems for a large cruise ship to meet new maritime regulations. Appl Energy 2018;211:306–17.
[2] Hansen JF, Wendt F, Lindtjørn JO. Fuel efficient power plant featuring variable speed generation system for DP drilling units. In: Proc. dyn. positioning conf.. 2016, p. 1–13.
[3] Hamilton J, Negnevitsky M, Wang X. The potential of variable speed diesel application in increasing renewable energy source penetration. Energy Procedia 2019;160:558–65.
[4] Fang S, Xu Y, Li Z, Ding Z, Liu L, Wang H. Optimal sizing of shipboard carbon capture system for maritime greenhouse emission control. IEEE Trans Ind Appl 2019;55(6):5543–53.
[5] Boveri A, Silvestro F, Molinas M, Skjong E. Optimal sizing of energy storage systems for shipboard applications. IEEE Trans Energy Convers 2018;34(2):801–11.
[6] Wen S, Lan H, Yu DC, Fu Q, Hong Y-Y, Yu L, et al. Optimal sizing of hybrid energy storage sub-systems in PV/diesel ship power system using frequency analysis. Energy 2017;140:198–208.
[7] Li Z, Xu Y, Fang S, Wang Y, Zheng X. Multiobjective coordinated energy dispatch and voyage scheduling for a multienergy ship microgrid. IEEE Trans Ind Appl 2019;56(2):989–99.
[8] Li Z, Xu Y, Fang S, Wang Y, Zheng X. Multiobjective coordinated energy dispatch and voyage scheduling for a multienergy ship microgrid. IEEE Trans Ind Appl 2019;56(2):989–99.
[9] Shang C, Srinivasan D, Reindl T. Economic and environmental generation and voyage scheduling of all-electric ships. IEEE Trans Power Syst 2015;31(5):4087–96.
[10] De A, Mamanduru VKR, Gunasekaran A, Subramanian N, Tiwari MK. Composite particle algorithm for sustainable integrated dynamic ship routing and scheduling optimization. Comput Ind Eng 2016;96:201–15.
[11] Huang Y, Lan H, Hong Y-Y, Wen S, Fang S. Joint voyage scheduling and economic dispatch for all-electric ships with virtual energy storage systems. Energy 2020;190:116268.
[12] De A, Choudhary A, Tiwari MK. Multiobjective approach for sustainable ship routing and scheduling with draft restrictions. IEEE Trans Eng Manage 2017;66(1):35–51.
[13] Kanellos FD, Tsekouras GJ, Hatziargyriou ND. Optimal demand-side management and power generation scheduling in an all-electric ship. IEEE Trans Sustain Energy 2014;5(4):1166–75.
[14] Wu Z, Xia X. Tariff-driven demand side management of green ship. Sol Energy 2018;170:991–1000.
[15] Shotorbani AM, Zeinal-Kheiri S, Chhipi-Shrestha G, Mohammadi-Ivatloo B, Sadiq R, Hewage K. Enhanced real-time scheduling algorithm for energy management in a renewable-integrated microgrid. Appl Energy 2021;304:117658.
[16] Çimen H, Bazmohammadi N, Lashab A, Terriche Y, Vasquez JC, Guerrero JM. An online energy management system for AC/DC residential microgrids supported by non-intrusive load monitoring. Appl Energy 2021;118136.
[17] Quan S, Wang Y-X, Xiao X, He H, Sun F. Real-time energy management for fuel cell electric vehicle using speed prediction-based model predictive control considering performance degradation. Appl Energy 2021;304:117845.
[18] Wang X, Atkin J, Bazmohammadi N, Bozhko S, Guerrero JM. Optimal load and energy management of aircraft microgrids using multi-objective model predictive control. Sustainability 2021;13(24):13907.
[19] Smogeli Ø, et al. Ventilated thrusters in dynamic positioning mode control of marine propellers from normal to extreme conditions. NTNU; 2006.
[20] Hou J, Song Z, Hofmann H, Sun J. Adaptive model predictive control for hybrid energy storage energy management in all-electric ship microgrids. Energy Convers Manage 2019;198:111929.
[21] Hou J, Song Z, Park H, Hofmann H, Sun J. Implementation and evaluation of real-time model predictive control for load fluctuations mitigation in all-electric ship propulsion systems. Appl Energy 2018;230:62–77.
[22] Hou J, Sun J, Hofmann H. Adaptive model predictive control with propulsion load estimation and prediction for all-electric ship energy management. Energy 2018;150:877–89.
[23] Xie P, Tan S, Guerrero JM, Vasquez JC. MPC-informed ECMS based real-time power management strategy for hybrid electric ship. Energy Rep 2021;7:126–33.
[24] Hou J, Sun J, Hofmann H. Control development and performance evaluation for battery/flywheel hybrid energy storage solutions to mitigate load fluctuations in all-electric ship propulsion systems. Appl Energy 2018;212:919–30.
[25] Jaurola M, Hedin A, Tikkanen S, Huhtala K. Topti:a flexible framework for optimising energy management for various ship machinery topologies. J Mar Sci Technol 2019;24(4):1183–96.
[26] Chua LW, Tjahjowidodo T, Seet GG, Chan R. Implementation of optimization-based power management for all-electric hybrid vessels. Ieee Access 2018;6:74339–54.
[27] Zhu J, Chen L, Wang X, Yu L. Bi-level optimal sizing and energy management of hybrid electric propulsion systems. Appl Energy 2020;260:114134.
[28] Planakis N, Papalambrou G, Kyrtatos N. Ship energy management system development and experimental evaluation utilizing marine loading cycles based on machine learning techniques. Appl Energy 2022;307:118085.
[29] Haseltalab A, Negenborn RR. Model predictive maneuvering control and energy management for all-electric autonomous ships. Appl Energy 2019;251:113308.
[30] Wu P, Partridge J, Bucknall R. Cost-effective reinforcement learning energy management for plug-in hybrid fuel cell and battery ships. Appl Energy 2020;275:115258.
[31] Wen S, Zhao T, Tang Y, Xu Y, Fang S, Zhu M, Ding Z. Joint energy management and voyage scheduling for all-electric ships using dynamic real-time electricity price of onshore power. In: 2020 IEEE/IAS 56th industrial and commercial power systems technical conference. IEEE; 2020, p. 1–8.
[32] Yuan Y, Zhang T, Shen B, Yan X, Long T. A fuzzy logic energy management strategy for a photovoltaic/diesel/battery hybrid ship based on experimental database. Energies 2018;11(9):2211.
[33] Chen H, Zhang Z, Guan C, Gao H. Optimization of sizing and frequency control in battery/supercapacitor hybrid energy storage system for fuel cell ship. Energy 2020;197:117285.
[34] Hasanvand S, Rafiei M, Gheisarnejad M, Khooban M-H. Reliable power scheduling of an emission-free ship: Multiobjective deep reinforcement learning. IEEE Trans Transp Electr 2020;6(2):832–43.
[35] Banaei M, Rafiei M, Boudjadar J, Khooban M-H. A comparative analysis of optimal operation scenarios in hybrid emission-free ferry ships. IEEE Trans Transp Electr 2020;6(1):318–33.
[36] Kalikatzarakis M, Geertsma R, Boonen E, Visser K, Negenborn R. Ship energy management for hybrid propulsion and power supply with shore charging. Control Eng Pract 2018;76:133–54.
[37] Hou J, Sun J, Hofmann HF. Mitigating power fluctuations in electric ship propulsion with hybrid energy storage system: Design and analysis. IEEE J Ocean Eng 2017;43(1):93–107.
[38] Kolmanovsky I, Sivergina I, Sun J. Simultaneous input and parameter estimation with input observers and set-membership parameter bounding: theory and an automotive application. Internat J Adapt Control Signal Process 2006;20(5):225–46.
[39] Zheng L, Zhou B, Cao Y, Or SW, Li Y, Chan KW. Hierarchical distributed multi-energy demand response for coordinated operation of building clusters. Appl Energy 2022;308:118362.
[40] Tan S, Xie P, Guerrero JM, Vasquez JC. False data injection cyber-attacks detection for multiple DC microgrid clusters. Appl Energy 2022;310:118425.
[41] Sulligoi G, Bosich D, Vicenzutti A, Khersonsky Y. Design of zonal electrical distribution systems for ships and oil platforms: Control systems and protections. IEEE Trans Ind Appl 2020;56(5):5656–69. http://dx.doi.org/10.1109/TIA.2020.2999035.

[42] Xie P, Guerrero JM, Tan S, Bazmohammadi N, Vasquez JC, Mehrzadi M, et al. Optimization-based power and energy management system in shipboard microgrid: A review. IEEE Syst J 2021.
[43] Van Vu T, Gonsoulin D, Diaz F, Edrington CS, El-Mezyani T. Predictive control for energy management in ship power systems under high-power ramp rate loads. IEEE Trans Energy Convers 2017;32(2):788–97.
[44] Vu T, Paran S, El Mezyani T, Edrington C. Real-time distributed power optimization in the DC microgrids of shipboard power systems. In: 2015 IEEE electric ship technologies symposium. IEEE; 2015, p. 118–22.
[45] Feng X, Butler-Purry KL, Zourntos T. Real-time electric load management for DC zonal all-electric ship power systems. Electr Power Syst Res 2018;154:503–14.
[46] Feng X, Butler-Purry KL, Zourntos T. Multi-agent system-based real-time load management for all-electric ship power systems in DC zone level. IEEE Trans Power Syst 2012;27(4):1719–28.
[47] Edrington CS, Ozkan G, Papari B, Gonsoulin DE, Perkins D, Vu TV, et al. Distributed energy management for ship power systems with distributed energy storage. J Mar Eng Technol 2020;19(sup1):31–44.
[48] Vu TV, Perkins D, Gonsoulin D, Edrington CS, Papari B, Schoder K, et al. Large-scale distributed control for MVDC ship power systems. In: IECON 2018-44th annual conference of the IEEE industrial electronics society. IEEE; 2018, p. 3431–6.
[49] Hossain MR, Ginn HL. Real-time distributed coordination of power electronic converters in a DC shipboard distribution system. IEEE Trans Energy Convers 2017;32(2):770–8.
[50] Lai K, Illindala MS. A distributed energy management strategy for resilient shipboard power system. Appl Energy 2018;228:821–32.
[51] Jalkanen J-P, Johansson L, Kukkonen J, Brink A, Kalli J, Stipa T. Extension of an assessment model of ship traffic exhaust emissions for particulate matter and carbon monoxide. Atmos Chem Phys 2012;12(5):2641–59.
[52] Satpathi K, Balijepalli VM, Ukil A. Modeling and real-time scheduling of DC platform supply vessel for fuel efficient operation. IEEE Trans Transp Electr 2017;3(3):762–78.
[53] Wheeler KR. Efficient operation of diesel generator sets in remote conditions (Ph.D. thesis), Virginia Tech; 2017.
[54] Zhang W, Li J, Xu L, Ouyang M. Optimization for a fuel cell/battery/capacity tram with equivalent consumption minimization strategy. Energy Convers Manage 2017;134:59–69.
[55] Wheeler KR. Efficient operation of diesel generator sets in remote conditions (Ph.D. thesis), Virginia Tech; 2017.
[56] Smogeli ØN. Control of marine propellers: from normal to extreme conditions. Fakultet for ingeniørvitenskap og teknologi; 2006.
[57] Minsaas KJ, Faltinsen OM, Persson B. On the importance of added resistance, propeller immersion and propeller ventilation for large ships in a seaway. 1983.
[58] Fang S, Xu Y, Li Z, Zhao T, Wang H. Two-step multi-objective management of hybrid energy storage system in all-electric ship microgrids. IEEE Trans Veh Technol 2019;68(4):3361–73.
[59] Shagar V, Jayasinghe SG, Enshaei H. Frequency transient suppression in hybrid electric ship power systems: A model predictive control strategy for converter control with energy storage. Inventions 2018;3(1):13.
[60] Fang R, Jiang W, Khan J, Dougal R. System-level thermal modeling and co-simulation with hybrid power system for future all electric ship. In: 2009 IEEE electric ship technologies symposium. IEEE; 2009, p. 547–53.
[61] Jiang Q, Hong H. Wavelet-based capacity configuration and coordinated control of hybrid energy storage system for smoothing out wind power fluctuations. IEEE Trans Power Syst 2012;28(2):1363–72.
[62] Jaurola M, Hedin A, Tikkanen S, Huhtala K. Topti a flexible framework for optimising energy management for various ship machinery topologies. J Mar Sci Technol 2019;24(4):1183–96.
[63] Gupta V. ECMS based hybrid algorithm for energy management in parallel hybrid electric vehicles. HCTL Open Int J Technol Innov Res (IJTIR) 2015;14.
[64] Chua LW, Tjahjowidodo T, Seet GG, Chan R. Implementation of optimization-based power management for all-electric hybrid vessels. IEEE Access 2018;6:74339–54.
[65] Hong Z, Li Q, Han Y, Shang W, Zhu Y, Chen W. An energy management strategy based on dynamic power factor for fuel cell/battery hybrid locomotive. Int J Hydrogen Energy 2018;43(6):3261–72.
[66] Boyd S, Parikh N, Chu E. Distributed optimization and statistical learning via the alternating direction method of multipliers. Now Publishers Inc; 2011.
[67] Vásquez CAM. Evaluation of medium speed diesel generator sets and energy storage technologies as alternatives for reducing fuel consumption and exhaust emissions in electric propulsion systems for PSVs. Cienc Tecnol Buques 2016;9(18):49–62.